Chapter 6

Spectroscopic Observations of UVX QSO Candidates

6.1 Introduction

In this chapter we describe preliminary spectroscopic observations of the UVX catalogue discussed in Chapter 4. Two separate investigations were undertaken to ascertain the effectiveness of the UVX catalogue at selecting QSOs. Observations were carried out using the 2-degree Field (2dF) (Taylor, 1995) and FLAIR-II (Parker & Watson, 1995) fibre-optic, multi-object spectroscopy systems at the AAT and UKST respectively.

First, the catalogue was sub-divided into a bright and a faint portion; the bright sample containing all UVX objects with b_J magnitude in the range $17.0 \leq b_J < 18.25$, while the faint sample covered the range $18.25 \leq b_J \leq 21.0$. The bright sample was observed using FLAIR, while for the faint sample the 2dF instrument was used. The primary aims of obtaining the FLAIR data were to reduce the amount of scattered light from bright objects in the 2dF spectrograph, and secondly, to test the effectiveness of the FLAIR system at obtaining QSO spectra. Below we will first discuss observations of the bright FLAIR sample, followed by the faint 2dF sample in Section 6.3. These sections will include a discussion of the various properties of the samples, including completeness and contamination rates. Our conclusions are given in Section 6.4.

This survey is still in progress, with further data being obtained during the writing of this thesis. The data presented here constitute a small fraction of the final sample, and have been primarily used to estimate the effectiveness of the survey. We also have the opportunity at this time to make improvements to the catalogue, based on the spectroscopic results in this chapter.

Table 6.1: Details of the FLAIR observations of QSO survey fields.

field name	RA (B1950)	Dec (B1950)	exposure time(s)	No. of QSO candidates
f411-b1	00 46 00	-30 00 00	8×3000	64
f469-b1	23 00 00	-30 00 00	9×3000	75

6.2 The Bright FLAIR QSO Sample

6.2.1 Observations and the FLAIR-II instrument

Two fields were observed using FLAIR over a period of 3 nights. The field f411-b1 was observed on the night of the 13/9/96, while the field f469-b1 was observed over the two nights 12-13/10/96 (Observers M. Hartley and K. Russell). Two plate holders are available to position fibres, the first with 73 fibres and the second with 92. The fibres are 6.7″ (100μm) in diameter. Field f411-b1 was observed with the first plate holder, while field f469-b1 used the second. FLAIR has a semi-manual fibre positioning system. Fibres are fed into a floor mounted (so highly stable) spectrograph. The FLAIR detector is a 400×578 thinned, back-illuminated EEV CCD, with a read-out noise of $\simeq 11e^-$ and a gain of $\simeq 1e^-$/ADU. A 250B grating was used giving a resolution of 6.3Å/pixel. Bias frames were taken at the beginning of each night, followed by mercury-cadmium (Hg-Cd) and neon (Ne) arcs. A number of 3000 second exposures were obtained on our survey fields, (see Table 6.1). On both fields a number of fibres (~ 10) were allocated to the night sky. At the end of the night further arcs were taken along with dome flat-fields. Observing conditions were bad, with cirrus and poor seeing, during the night of the 13/9/96 (f411-b1 field).

6.2.2 FLAIR data reduction

The FLAIR data were reduced using the IRAF astronomical reduction package according to Drinkwater & Holman (1996) . The object, flat-field and arc frames were de-biased, overscan corrected and trimmed using the **imred.ccdred.ccdproc** task. Flat-fields were then median combined using **flatcombine**, with a 4σ clipping to remove CREs. The Hg-Cd and Ne arcs taken at the beginning of the night were added together using **imarith**, those taken at the end of the night were combined separately. The object frames were averaged together in groups of 2 or 3 using **imcombine**. The algorithm CRREJECT was used with a high threshold $\simeq 7\sigma$ in order to remove CREs. This threshold removes almost all of the CREs while not removing any real data from the spectra. The frames were combined in groups of 2 or 3, so that images combined together have similar seeing, and there is not a significant shift in the position of the spectra. The final reduced spectra can then be summed at a later stage.

Spectral extraction was performed using the **imred.specred.dofibers** package. This is a multi-task package which automatically traces each fibre aperture along the CCD and extracts the spectra. It then extracts the flat-field spectra and uses these, summed in the dispersion direction, to normalize the fibre throughput. The next stage is to wavelength calibrate the spectra. **dofibers** matches the arc lines to an input list of line wavelengths and produces a polynomial fit to each individual arc spectrum. These fits are then used to wavelength calibrate the object spectra. Finally, **dofibers** median combines the sky spectra and subtracts the composite sky spectra from the object spectra.

This process resulted in set of sky subtracted, wavelength calibrated, object spectra; spectra of the same object were then combined using the **scombine** task.

6.2.3 Spectroscopic results

We now discuss the spectra obtained from the FLAIR observations. The spectra were identified by eye using the `REDSHIFT` program written by Dr. K. Glazebrook. The stellar spectra were classified according to an approximate spectral type. Objects which were possible QSOs, but did not show definite broad emission lines were classified as QSO?. The quality of QSO redshifts were also categorized; (1) signifies a certain redshift with two or more strong lines, (2) signifies a probable redshift with one strong line and one or more low signal-to-noise lines, (3) signifies an uncertain redshift, with only one strong line or only low signal-to-noise lines. This should be only be taken as a guide, as QSOs which show only Mg II emission were generally classified as having a class (1) redshift.

Table 6.2 shows the composition of the FLAIR sample. A total of 139 FLAIR spectra were obtained from the two pointings. We discuss the galactic and non-galactic components of the sample below. We should first note that the total number of candidates in the f411 and f469 fields is 76 and 158 respectively, so less than half of the QSO candidates in the f469 field were observed, candidates which were observed being chosen at random. The difference in the number of candidates in the two fields is due to several effects. Photometric zero-point errors and the position of f469 closer to the galactic plane contribute to this difference. The dominant effect however, appears to come from the broadening of the stellar locus at bright magnitudes in f469 (see Fig. 4.7).

Galactic stars

The majority of objects identified are found to be halo subdwarfs. Most lie in the spectral classification range $\sim A0$ to $G5$, although 2 are identified as K stars. All

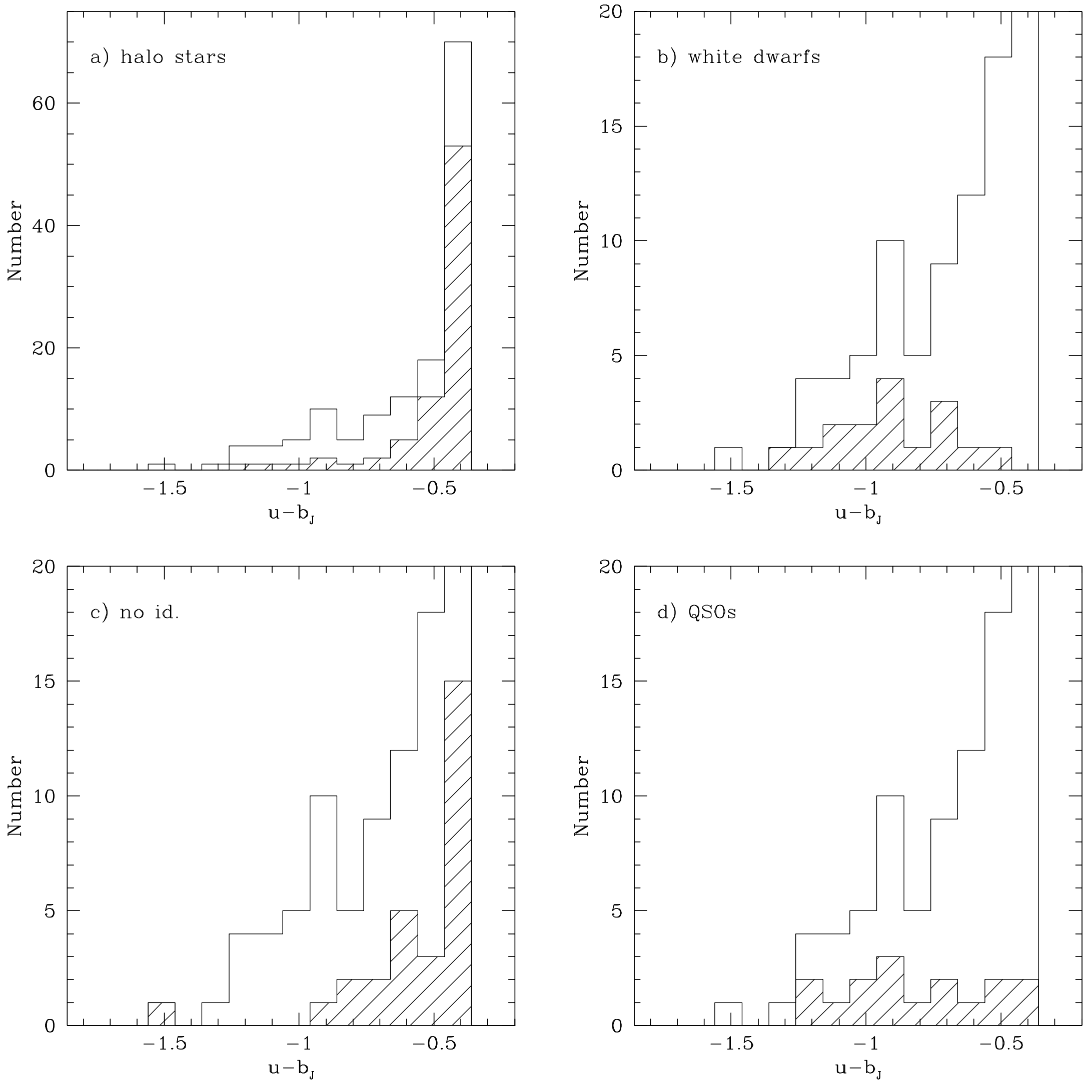

Figure 6.1: Histograms of the colour distribution of the components of the FLAIR sample. The shaded histograms show the distributions for the a) halo stars, b) white dwarfs, c) objects with no identification and d) QSOs respectively. The unshaded histogram in each case is for reference and shows the colour distribution of all observed objects. The two CVs are included in the white dwarf plot and the one QSO? ($u - b_{\rm J} = -0.53$) is included in the QSO plot.

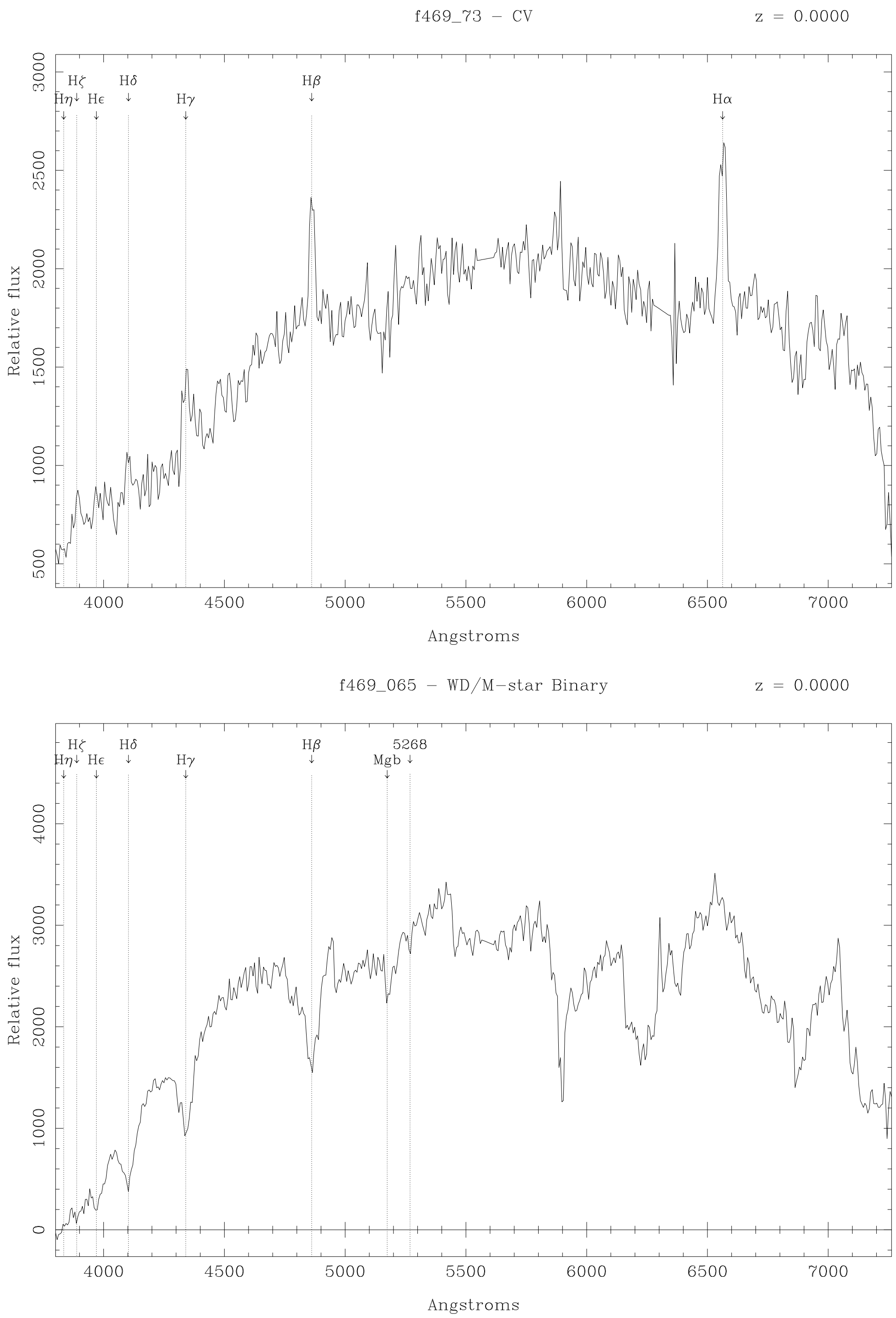

Figure 6.2: FLAIR spectra of a cataclysmic variable (top) and a DA white dwarf/M-star binary system (bottom).

Table 6.2: The composition of the FLAIR bright QSO sample.

	Number		
Identification	f469	f411	**Total**
subdwarf	53	25	**78**
White dwarf	8	7	**15**
CV	1	1	**2**
QSO	7	8	**15**
BAL QSO	0	0	**0**
QSO?	0	1	**1**
NL Galaxy	0	0	**0**
No id.	6	23	**29**
Total	75	64	**139**

these objects would generally be expected to have colours of $U-B \sim 0$ or redder, so are likely to have been added into the sample through photometric errors. The colour distribution of halo stars, shown in Fig. 6.1a, is strongly peaked at the red limit of our selection, demonstrating that these stars do not in any way form a complete sample. Almost all the remaining stars (15) are white dwarfs (WD). Fig 6.1b shows that these objects have blue colours and are therefore likely to form a complete sample. 12 of these show only hydrogen Balmer absorption lines and therefore belong to the DA class of white dwarfs. Of these, two objects f411_075 and f469_046 show evidence of core emission or line splitting in Hβ (f411_075 and f469_046), Hγ (f411_075) and Hδ (f411_075). This is possibly Zeeman splitting induced by strong magnetic fields, although the signal-to-noise is not sufficient to measure the effect. The remaining 3 WDs comprise a DAO WD, showing evidence of He II absorption, a DAB WD with neutral Helium absorption lines and one peculiar object showing broad hydrogen Balmer lines at the blue end of the spectrum ($\lambda < 5000$Å), but molecular absorptions bands at the red end of the spectrum (Fig. 6.2), usually associated with an M class star. This is most likely to be a WD(DA)/M-star binary system. Finally, we find two stellar objects with hydrogen Balmer emission lines. These are cataclysmic variables (CVs), which are accreting white dwarfs, and have colours similar to that of WDs (see Fig. 6.2).

QSOs

We find 15 QSOs in the two fields and one further QSO? object; spectra and details of these are listed in Appendix A. Their colour distribution is shown in Fig. 6.1d. Of the 15 confirmed QSOs only one is outside of the redshift range $0.3 < z < 2.2$. The magnitude and redshift distributions of these objects are shown in Fig. 6.3. We will show and discuss a combined number-magnitude relation for the FLAIR

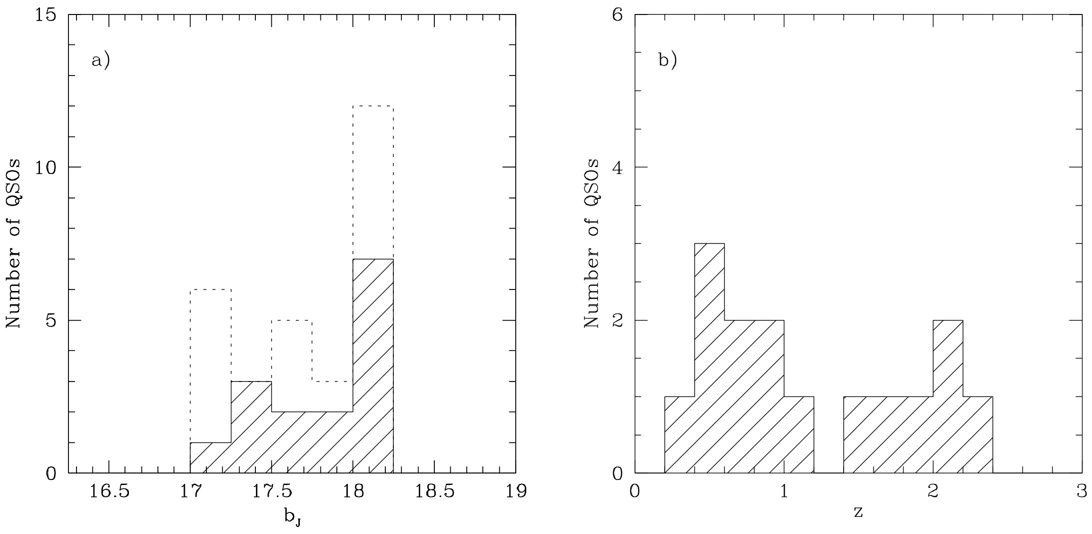

Figure 6.3: Distribution of QSOs in the FLAIR sample as a function of a) magnitude and b) redshift. The shaded histogram shows the QSO distributions in both cases. The dotted histogram in a) shows the distribution of unidentified sources.

and 2dF samples in Section 6.3.4. The redshift distribution is weighted towards low redshift, as we would expect in a bright QSO sample (see the LBQS $N(z)$ in Fig. 3.1). The LBQS (Hewett et al., 1995) shows a surface density of QSOs of 0.90 deg^{-2} between $b_{\rm J} = 17.0$ and 18.25, over the redshift range $0.3 < z < 2.2$. Considering the fraction of candidates observed in each field we find that the *effective* areas of the two fields are 20.86 and 10.62 deg^2 for the f411 and f469 fields respectively. The density of QSOs we find over the range $0.3 < z < 2.2$ is therefore 0.44 ± 0.12 QSOs per sq. deg, a factor of 2 less than found in the LBQS, with f411 and f469 having densities of 0.34 ± 0.13 and 0.66 ± 0.25 deg^{-2} respectively.

The LBQS has been shown to be extremely effective at selecting QSOs (Hewett et al., 1995) and there are several reasons for our lower density. First, even in this magnitude range we expect $\sim 10 - 15\%$ incompleteness from photometric errors and variability (due to our relatively blue UVX selection threshold). Second, a high fraction of these bright QSOs are found at low redshift. The UVX selection technique is not so effective at low redshift as these objects become both redder than the QSOs at higher redshift and are no longer classified as point sources; both these effects being primarily due to the increasing effect of the host galaxy at low redshift. Third, it is of course possible that there is a residual offset between the LBQS and 2dF $b_{\rm J}$ magnitude systems, which could cause this difference in number density. An offset of 0.1 mag could cause a 20% reduction in the measured QSO density.

We note that the f469 field QSO density is within 1σ of the expected value from the LBQS. The f411 field, which shows a particularly low density of QSOs, contains a high number of unidentified spectra. Over one third of the spectra could not be positively identified, these being mostly at the faint end of the sample where a higher fraction of QSOs is expected (as demonstrated in Fig. 6.3). There are 16 previously known QSOs in the f411 field which lie in the redshift and magnitude intervals $0.3 < z < 2.2$ and $17.0 < b_J < 18.25$. Of these, two are classed as merged objects on the APM scans and are not included in the survey (both are at low redshift, $z \sim 0.3 - 0.4$). One further object is slightly too red to fall within our colour selection (with $u - b_J = -0.35$). Of the remaining 13 QSOs we have obtained spectra of 11 with FLAIR. Of these we classify 6 as certain QSOs, one as QSO? and four have no identification. If we include these objects in our calculation of QSO surface density we find the f411 density to be 0.58 ± 0.17 deg^{-2} (for $0.3 < z < 2.2$), a number much more consistent with the f469 field and closer to the LBQS result. The f469 data show that the UKST/FLAIR, with adequate observing conditions, can obtain $> 90\%$ identifications from our UVX catalogue. This combination can obtain QSO densities consistent with the LBQS.

6.3 The Faint 2dF QSO Sample

6.3.1 Observations with the 2-degree Field instrument

The 2-degree Field instrument is a multi-fibre spectroscopic system which utilizes the wide field of view provided by a 4-component optical corrector. The corrector produces a field of two degrees diameter with some cost in terms of broad band imaging quality. However, for multi-fibre spectroscopy with fibres of $\sim 2''$ diameter ($2.16''$ at the field centre, $2.0''$ at the edges), the small loss due to variations across the field (mostly due to a Chromatic Variation in Distortion), is more than compensated by the increased field of view. There are two field plates onto which the fibres are positioned using a robotic positioner and magnetic buttons. The two field plates provide a substantial reduction in overheads by allowing the positioner to reconfigure one field while the other is being observed. 400 fibres can be positioned on each field, with two identical spectrographs receiving 200 fibres each. The spectrographs use thinned 1024×1024 Tektronix CCDs and there are a variety of low and medium resolution gratings available. Further details of the instrument can be found in the 2dF user manual (Bailey, 1996).

Our observations were carried out during a time of science verification testing. At this time the instrument had only 200 fibres per plate and one spectrograph with an engineering grade CCD (with diminished blue response). We use the 300B grating which has a dispersion of 178.8Å/mm. In order to make effective use of telescope time we combine our observations with those of the 2dF Galaxy Redshift Survey Project. Thus on average each field of 400 fibres will contain ~ 135 fibres observing QSO candidates, ~ 245 fibres observing galaxies and a further ~ 20 fibres on blank sky positions. In the current mode (only 200 fibres) we observe ~ 65 QSO candidates per 2dF pointing. We observed 7 individual fields, 4 were in the Southern (SGP) strip and 3 were in the Northern (NGP) strip. One field (NGP298) contained 3 very bright, $b_J \sim 9$ mag, stars which had been mis-classified as galaxies by the 2dF Galaxy Survey team. Contamination by these objects caused approximately half of

Table 6.3: Details of the 2dF observations of QSO survey fields.

UKST field	field name	RA (B1950)	Dec (B1950)	exposure time(s)	No. of QSO candidates	comments
f417	SGP238	03 08 43.8	-27 42 01	2×1800	26	
f417	SGP463	03 11 31.8	-32 11 58	3×1800	50	
f417	SGP392	03 12 51.9	-30 42 15	2×1800	70	
f853	NGP298	09 53 27.3	+00 23 56	3×1800	72	Bright stars
f853	NGP242	09 56 36.7	-00 56 40	3×1800	69	270R grating
f854	NGP361	10 11 03.6	+01 44 38	3×1800	59	low S/N
f466	SGP246	21 44 36.5	-29 12 20	4×1800	73	

the spectra to be unusable in this field. Another field (NGP242) was observed using the 270R grating rather than the 300B. Table 6.3 gives details of these observations. While the Southern fields used the catalogue limits described in Chapter 4, the Northern fields used a somewhat brighter, $b_J = 20.75$, magnitude limit with a redder selection limit of $u - b_J = -0.3$. The aim of these fields was to help assess the effect that altering our survey limits has on completeness and contamination.

For each field a number of 1800s exposures were taken of the candidate objects. As well as these, helium-neon-copper-argon arc exposures where taken, usually at both the beginning and end of a run of object exposures. Dome flats were taken to measure the individual fibre throughputs using a quartz lamp. Approximately 20 fibres were given over to blank sky positions for each field.

6.3.2 2dF data reduction

An eventual goal of the 2dF facility is to have a pipe-line processing system which will produce fully reduced spectra. At the time of this thesis the pipe-line software was still in the development stage, therefore the **IRAF dofibers** task was used to perform the spectroscopic data reduction. This task is described above in Section 6.2.2, and here we will outline points which are peculiar to the 2dF data set. First, the spectrograph is located on the top end ring of the telescope. While reducing losses due to long lengths of optical fibre this makes the instrument less stable than the FLAIR spectrograph. Therefore, it is not straightforward to combine multiple exposures taken at different times, due to non-linear shifts in the relative positions of the spectra. In cases where this is a problem we have combined our object spectra after extraction rather than before. This method has the disadvantage of being less effective at CRE rejection. In practice, for all fields where shifts in spectra positions were a significant problem, we had at least 3 exposures from which a median could be taken to remove CREs. A second point is that the current CCD has several cosmetic

Table 6.4: The composition of the 2dF QSO sample. The numbers of objects identified are listed for individual UKST fields and for the SGP (f417 and f466) and NGP (f853) samples.

	Number			
Identification	f417	f466	**SGP**	**NGP**
subdwarf	10	20	**30**	**44**
White dwarf	8	2	**10**	**1**
CV	1	1	**2**	**0**
QSO (inc. BALs)	82	32	**114**	**38**
BAL QSO	3	1	**4**	**0**
QSO?	2	1	**3**	**2**
NL Galaxy	25	11	**36**	**6**
No id.	18	6	**24**	**19**
Total	146	73	**219**	**110**

defects including bad columns. These were interpolated across using the task **fixpix**, and a note was made of these columns in the arc spectra so any line which contained cosmetic defects was not used to calculate the wavelength calibration.

6.3.3 Spectroscopic results

A total of 419 spectra have been obtained from the seven fields listed in Table 6.3, this includes 31 spectra which were contaminated by scattered light from the bright stars in the NGP298 field, leaving 388 spectra. We analyse the data from the Northern and Southern fields separately.

In the four SGP fields we obtained a total of 219 spectra of UVX QSO candidates. Identification was carried out by eye using the `REDSHIFT` program and spectra were classified as described in Section 6.2.3. In the 3 NGP fields we obtained 200 spectra. Field NGP361 has low signal-to-noise and, due to poor observing conditions, less than half the spectra could be classified; this field was left out of the following analysis. The 31 spectra contaminated by scattered light from the three bright stars were also removed from the sample leaving a total of 110 spectra in the two remaining NGP fields. The compositions of the SGP and NGP samples are shown in Table 6.4 and below we discuss the individual components of these samples.

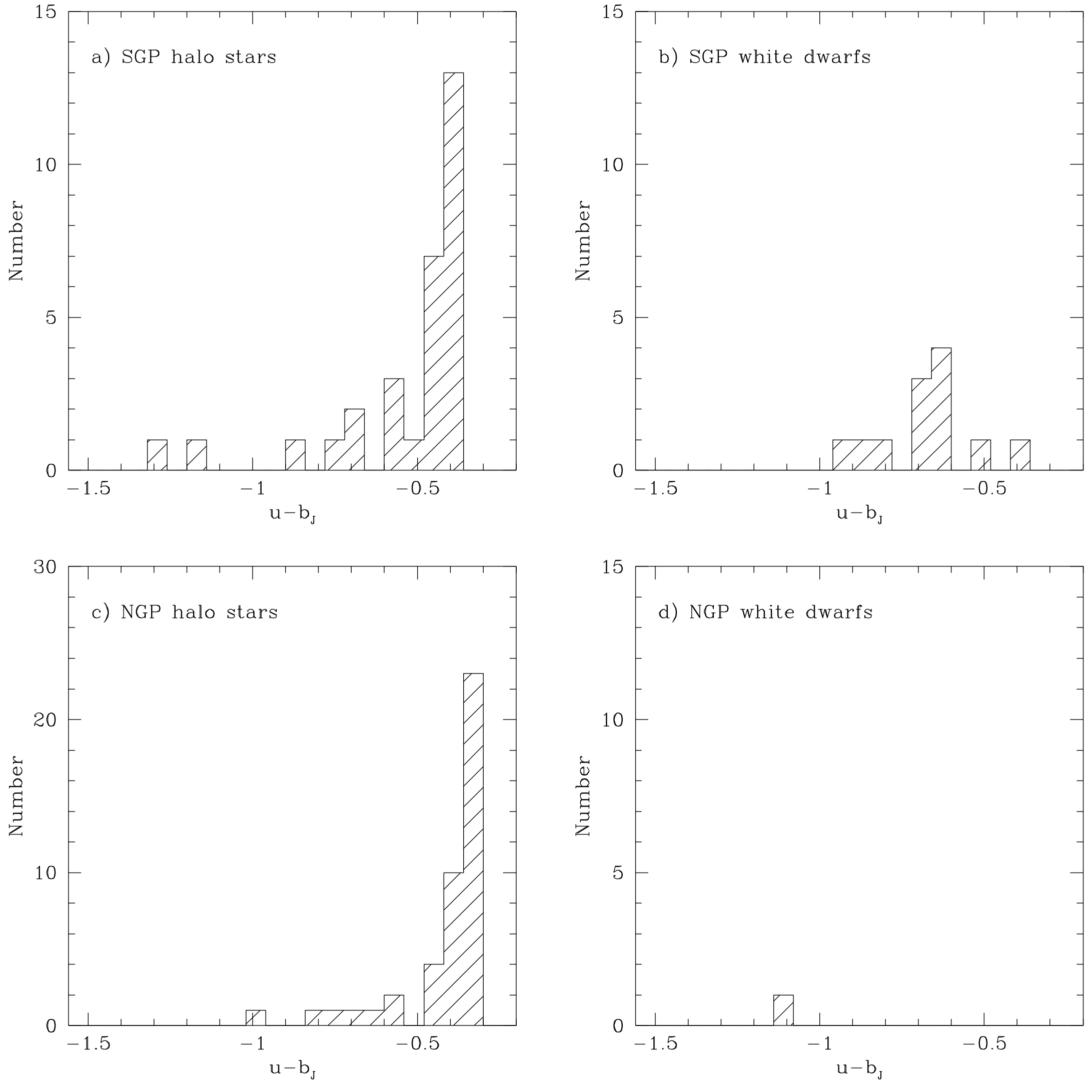

Figure 6.4: Colour distribution of stars found in the 2dF samples. a) SGP halo stars, b) SGP white dwarfs, c) NGP halo stars and d) NGP white dwarfs.

Galactic stars

Out of a total of 219 spectra the SGP sample contains 42 stellar objects, the majority of these (30 objects, 15% of the 195 classified spectra) being galactic halo subdwarfs in the range $\sim A0 - G5$. Fig 6.4 shows that the majority of halo stars are close to the red limit of our selection, as in the brighter FLAIR sample. Ten of the remaining stars are WDs, mostly of the DA variety, easily recognizable from their broad hydrogen Balmer lines. Two of these WDs appear to be of the rarer DAB type, which have weak HeI lines present in their spectra. The remaining two galactic sources are CVs. The 24 unclassified spectra comprise faint objects with low signal-to-noise, these being mostly located near the faint limit of our survey, or objects which show a strong continuum flux with no emission or absorption features visible. Many of these are likely to be subdwarfs as these objects are by far the most difficult to classify, generally having only weak absorption lines. The remaining continuum sources could be BL Lac objects, or possibly DC (continuum) WDs.

In the NGP fields we find a significantly higher fraction of halo subdwarfs, as expected, given the redder limits. There are 44 (48%) subdwarfs out of a total of 91 classified spectra. The vast majority of these appear to be A, F and G stars although in the NGP242 field, for which the 270R grating was used, stellar classification is more difficult since the Ca II H and K lines are not visible. We find two objects which appear to be WD/M-star binaries in the NGP242 field, although the R270 grating only allows us to see the Hβ absorption feature. One normal DA white dwarf was found in the NGP sample. Of the 44 subdwarfs, 22 have $u - b_{\rm J}$ colours between –0.36 and –0.3, thus the stellar contamination is doubled by moving the colour limit 0.06 mag redder.

QSOs and emission line galaxies

The SGP sample of 219 spectra resulted in the identification of 114 QSOs (excluding 2 QSO?s). The QSO spectra and details of individual objects are given in Appendix B. All of the QSOs were identified on the basis of their broad ($> 1000{\rm kms}^{-1}$) emission lines, particularly the Mg II(λ2798Å), C III](λ1909Å), C IV(λ1549Å) and Lyα+N V(λ1240Å) lines. The lowest redshift QSOs could also be identified by their broad Balmer emission lines. Several other weaker lines were also observed in a number of spectra, including the Si IV(λ1397Å), C II(λ2326Å) and [Ne V](λ3426Å) lines. Here we will discuss a number of objects of particular interest. The lowest redshift QSO is TQ392_258 at a redshift of 0.213. This object has an apparent magnitude of $b_{\rm J} = 20.99$, and is therefore the faintest object in the catalogue with an absolute magnitude of $M_{\rm b_J} = -19.54$ (throughout this section we will assume $H_0 = 50{\rm kms}^{-1}{\rm Mpc}^{-1}$ and $\Omega_0 = 1$). The absolute magnitude in the $b_{\rm J}$ band, $M_{\rm b_J}$, is found using

$$M_{\rm b_J} = b_{\rm J} - 5\log(d_L) + 2.5(1+\alpha)\log(1+z) - 25 \qquad (6.1)$$

where d_L is the luminosity distance to the QSO, which for $\Omega_0 = 1$ is given by

$$d_L = \frac{2c}{H_0}[(1+z) - (1+z)^{1/2}] \tag{6.2}$$

For the K-correction we use a spectral slope of $\alpha = -0.5$. A further 12 objects have $M_{\rm b_J} > -23$, all below $z = 0.8$. Therefore 11% of the QSO sample could be classified as Seyferts. The highest redshift QSO is at $z = 2.684$ and has $b_{\rm J} = 18.53$, implying an absolute magnitude of $M_{\rm b_J} = -27.39$, the most luminous source in the sample. Five QSOs show broad absorption line (BAL) features with evidence of broad absorption in Mg II, C IV and Lyα+N V. These objects comprise $4.3 \pm 2.0\%$ of the total sample, consistent with previous QSO surveys (Boyle et al., 1990). Several of the highest redshift QSOs show Lyα absorption at redshifts below that of the QSO. TQ462_271 ($z = 2.684$) and TQ463_254 ($z = 2.667$) are the most prominent examples, and merit further investigation with high resolution spectroscopy to measure the redshifts and hydrogen columns of the absorbing systems.

As well as QSOs, 36 narrow emission line (NL) galaxies were found in this sample. These objects show strong hydrogen Balmer, [O II](λ3727Å) and [O III](λ4959Å, λ5007Å) lines, indicators of significant star formation. The majority of these objects are red, $u - b_{\rm J} > -0.5$, and faint, $b_{\rm J} > 20.6$, and range in redshifts from $z \sim 0.1$ to ~ 0.5. These objects are small compact star-forming galaxies which have been classified as stars in our analysis; their relatively red colours suggest that this sample of galaxies is likely to be highly incomplete. NL galaxies form 18% of the classified sample, compared to 4% found in the Durham/AAT QSO survey (Boyle et al., 1990). This discrepancy is partly due to the differing magnitude limits of the two samples, as most narrow line galaxies are found near to the faint limit of the survey. We note in Chapter 4 that the 2dF QSO survey limit of $b_{\rm J} = 21$ mag is, on average, slightly deeper (by ~ 0.25 mag) than the Durham/AAT sample. 22 of the NL galaxies were found fainter than $b_{\rm J} = 20.75$.

The NGP fields contain 40 objects classified as QSOs, two of which are QSO?s. These QSOs range in redshift from $z = 0.235$ to 2.558. No BAL QSOs are found in this sample, which is consistent with the fraction found in the SGP sample. Four QSOs (11%) have absolute magnitudes fainter than $M_{\rm b_J} = -23.0$ and so would be classified as Seyferts. The NGP sample contains fewer narrow line galaxies the SGP sample; only 6 are identified. Using common selection criteria, $b_{\rm J} \leq 20.75$ and $u - b_{\rm J} \leq -0.36$, the SGP sample would contain 14 (9%) NL galaxies while the NGP sample would contain only 3 (4%).

6.3.4 Properties of the QSO sample

We now go on to look at the statistical properties of the 2dF QSO sample, in order to ascertain the completeness of the sample and compare it to other QSO surveys. First, the redshift distributions, $n(z)$, of the SGP and NGP samples are shown in Fig 6.5. Overplotted on the redshift distributions is a polynomial fit to the Durham/AAT sample (Shanks & Boyle, 1994) normalized to the numbers of QSOs

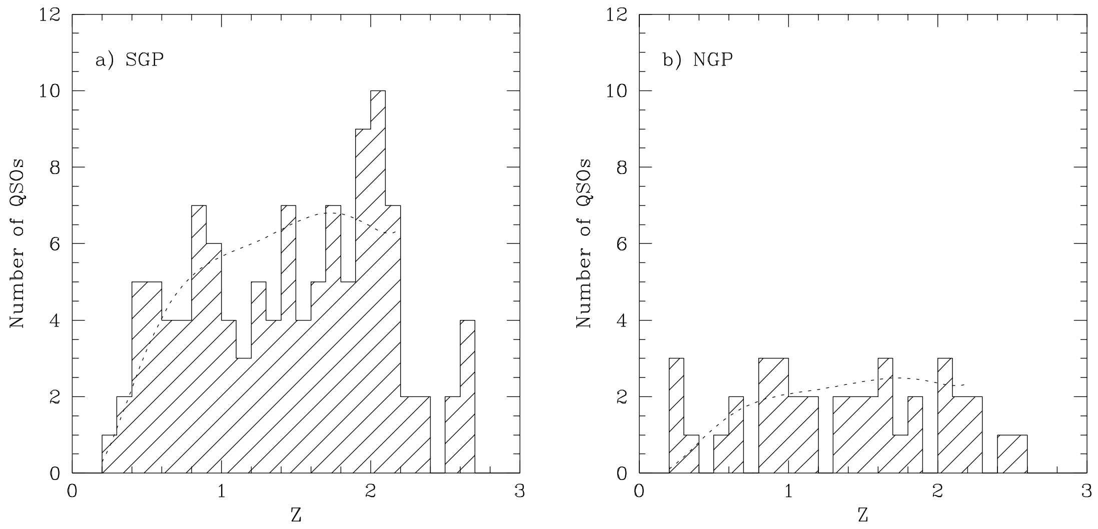

Figure 6.5: The distribution of QSOs as a function of redshift in the a) SGP and b) NGP samples. The dotted lines show a polynomial fit to the Durham/AAT sample at $z < 2.2$ normalized to the number of QSOs in each sample.

Table 6.5: Number densities of QSOs in individual UKST fields. Densities are given in $\deg^{-2}$.

field	No. of cands.	effective area	No. of QSOs	No. of QSOs $0.3 < z < 2.2$	QSO density	QSO density $0.3 < z < 2.2$
f417	146	2.55	82	73	32.2 ± 3.6	28.6 ± 3.4
f466	73	0.85	32	30	37.5 ± 6.6	35.2 ± 6.4
f853	110	2.11	38	31	18.0 ± 2.4	14.7 ± 3.0

in each plot. A χ^2 test comparing the SGP and NGP to the Durham/AAT survey finds reduced χ^2 of 0.63 and 0.58 for the SGP and NGP respectively. The most noticeable feature of the $n(z)$ is the sudden fall off at $z = 2.2$, expected due to the changing colours of the QSO population near this redshift.

We calculate the surface number density of QSOs in both the samples. The SGP data is taken from 2 different UKST field areas, f466 and f417. The limiting magnitudes in the two fields were $b_J = 21.06$ and $b_J = 20.92$ for f466 and f417 respectively (the difference is due to plate-edge zero point corrections being used). Each 2dF pointing only observed a fraction of the UVX candidates within the 2° diameter field, due to the collaboration with the 2dF Galaxy Redshift Survey and only having 200 fibres available. We therefore calculate the effective area of each 2dF pointing based on the fraction of UVX candidates observed. The effective areas for each field, along with the calculated QSO densities, are given in Table 6.5.

The f466 field shows the highest number density of QSOs at 37.5 ± 6.6 deg^{-2}, while the f417 field has a lower density of 32.2 ± 3.6 deg^{-2}. In order to compare the two fields, we reject all QSOs fainter than $b_J = 20.92$. The number density in f466 then becomes 32.8 ± 6.2 or 30.5 ± 6.0 ($0.3 < z < 2.2$), which is more consistent with the values found in the f417 field. Combining the f466 and f417 fields at this limit we have 110 QSOs (99 within $0.3 < z < 2.2$) in an effective area of 3.40 deg^2 which is then a surface density of 32.3 ± 3.1 or 29.1 ± 2.9 ($0.3 < z < 2.2$) deg^{-2}. $b_J = 20.92$ is equivalent to $b = 21.17$ (b being the magnitude system used in the Durham/AAT QSO Survey). The number density of QSOs found in the Durham/AAT sample was 36.7 deg^{-2} at a limit of $b = 21$. The slope of the integrated number counts in this region is ~ 0.28 (Boyle et al., 1988b) and therefore we expect 40.9 deg^{-2} at $b = 21.17$. So we appear to be selecting only $71.1 \pm 7.1\%$, which is lower than, but not inconsistent with, the $\sim 80\%$ predicted in Chapter 4. At $b_J = 21$ this completeness corresponds to a QSO density of 30.6 deg^{-2}, compared to ~ 34 deg^{-2} estimated from previously known QSOs.

Before we discuss this result any further we will similarly analyse the NGP data, which have a brighter magnitude limit, $b_J = 20.75$, and a redder colour selection, $u - b_J = -0.3$. Table 6.5 contains the calculated QSO density in the NGP f853 field. The number density of QSOs, at 18.0 ± 2.4 deg^{-2} (and 14.7 ± 3.0 for $0.3 < z < 2.2$), is lower than the SGP data, where the density is 28.5 ± 2.9 (26.2 ± 2.8 for $0.3 < z < 2.2$) for $b_J < 20.75$. It is also below the number density found in the Durham/AAT survey, which is 36.7 deg^{-2} at this limit.

More information regarding the expected completeness of the sample can be obtained from analysis of the colour distribution of the identified QSOs (shown in Fig. 6.6). The distribution peaks bluer than our UVX limit, which allows us to fit a Gaussian profile to the colour distribution of SGP QSOs over the range $0.3 < z < 2.2$. Integrating this function to the colour selection limit of $u - b_J = -0.36$ we find that 85.1% of QSOs should be selected, under the assumption, of course, that the Gaussian distribution is a reasonable description of the data. This number is much more consistent with the expected completeness obtained in Chapter 4. Three QSOs in the NGP data set have colours $u - b_J > -0.36$, two of which are within the redshift range $0.3 < z < 2.2$. They therefore constitute $7.9 \pm 4.6\%$ or $6.5 \pm 4.6\%$ ($0.3 < z < 2.2$) of the total NGP sample, whereas from the Gaussian fit to the SGP data we would expect this to be 3.8%, which, considering the large error, is obviously consistent.

We can combine the FLAIR and 2dF data sets to construct the differential number magnitude relation for our sample; this is shown in Fig. 6.7 and compared to the LBQS and Durham/AAT surveys. The data clearly show the break in the number-magnitude relation at $b_J \simeq 19$, which is present in the LBQS and Durham/AAT data, but also shows an under-density compared to these surveys. Our analysis of previously known QSOs in Chapter 4 predicts a completeness of $\sim 80\%$, where the incompleteness is due to photometric errors and variability. The QSO density measured from spectroscopic data in the SGP region is consistent with this. The NGP data show significantly lower QSO densities, but these data in particular are of vari-

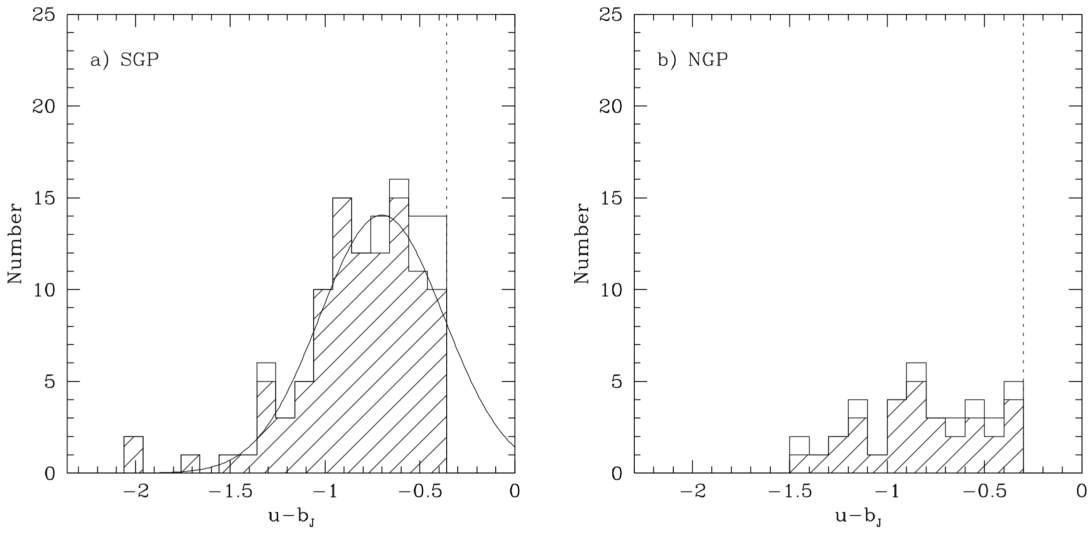

Figure 6.6: The distribution of QSOs as a function of $u - b_J$ colour for a) the SGP and b) the NGP samples. The shaded histograms show QSOs in the redshift range $0.3 < z < 2.2$ while the unshaded histogram includes those QSOs detected outside of these redshift limits. The dotted lines show the colour selection limits in each case (-0.36 for the SGP fields and -0.3 for the NGP fields). Note that the bins in the two plots are offset with respect to one another by 0.06 mag so as to make the bin nearest to the colour limit complete. a) shows a Gaussian fit (peak at -0.7 and width 0.328) to the colour distribution of QSOs within $0.3 < z < 2.2$.

able quality (17% of candidates were not identified). Further data, currently being obtained using the 2dF facility, should produce a more uniform data set. The levels of completeness determined here and in Chapter 4 drive a continued investigation, aimed at improving the candidate catalogue used in the 2dF QSO Survey. Below, in our conclusions, we will outline one possible way to make these improvements.

6.4 Conclusions

We have made preliminary spectroscopic observations of UVX QSO candidates from the UVX catalogue discussed in Chapter 4. The observations have been carried out using both the 2-degree Field facility at the AAT and the FLAIR system at the UKST. Bright ($17 < b_J < 18.25$) candidates were observed using FLAIR and fainter ($18.25 < b_J < 21.0$) candidates were observed using 2dF. 139 spectra were obtained from FLAIR and 419 from 2dF. The aim of this investigation was to test the effectiveness of the UVX catalogue at selecting QSOs, in terms of both completeness and contamination.

As well as QSOs, the samples also contain significant numbers of both galactic stars and narrow emission line galaxies. The galaxies lie at the faint and red limits of the sample and as such form a highly incomplete sample. This is also the case for

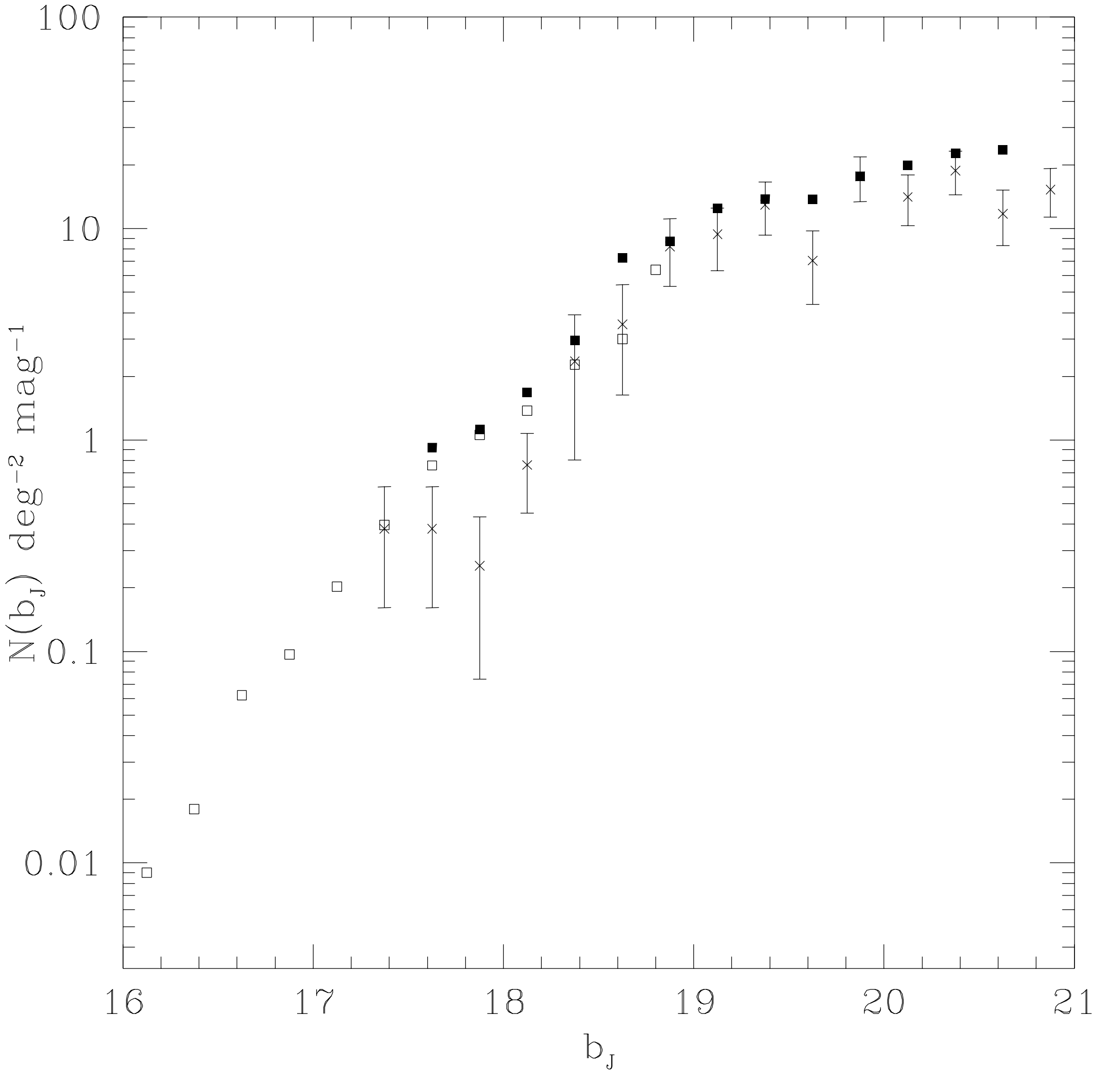

Figure 6.7: The number magnitude relation for the combined FLAIR and 2dF (SGP only) data (crosses). The points without errors are the LBQS (open squares) and the Durham/AAT (filled squares) survey. The Durham/AAT survey has been converted from the b magnitude system to $b_{\rm J}$ using the conversion in Eq. 4.10.

the majority of galactic stars, which are halo subdwarfs (A, F and G stars) scattered into our colour limits by photometric errors. Apart from these objects we also find 28 hot white dwarfs, which due to their bluer colours do form a complete sample. Most of these objects are DA white dwarfs, dominated by broad hydrogen Balmer lines. Four of these objects show evidence of helium absorption, either neutral (DAB WDs) or ionized (DAO). Three of the WDs show broad molecular absorption features at $\sim 6000 - 7000$Å, these are WD/M-star binary systems. Four CVs were also found, being easily distinguishable by their hydrogen Balmer emission lines. The number of WDs found implies that the completed survey will contain ~ 2000 WDs, which will be invaluable to the study of galactic structure.

The combined data set found a total of 167 QSOs. In particular the SGP subsample of the 2dF observations contains 114 QSOs, that is 50% of the sample were positively identified as QSOs. The contamination comes mainly from halo subdwarfs at bright magnitudes, but at fainter magnitudes, $18.25 \leq b_{\rm J} \leq 21.0$, we find approximately equal numbers of NL galaxies and subdwarfs. The increased number of NL galaxies is most likely to be due to the star-galaxy separation becoming less accurate at $b_{\rm J} \sim 21$. The use of a faint limit of $b_{\rm J} = 20.75$, and a colour limit of $u - b_{\rm J} \leq -0.3$ reduces the number of NL galaxies but increases the number of subdwarfs, so that the total contamination is greater.

Exact quantitative analysis of the amount of incompleteness is vital in assessing the effectiveness of the 2dF QSO survey. This is somewhat hindered by the inhomogeneous nature of the current data, particularly in the case of the currently available data in the NGP region of the survey and the f411-1b FLAIR data. Given the measured densities of QSOs, the *current estimates* suggest a completeness in the SGP of $71.1 \pm 7.1\%$, which corresponds to a QSO surface density at $b_{\rm J} = 21$ of ~ 30 deg^{-2}.

These levels of completeness give a QSO density which is lower than expected. We would like a high QSO density as the statistics of QSO clustering are strongly dependent on the density of QSOs in the sample. From Chapter 4 we aimed for $\sim 80\%$ completeness (~ 35 deg^{-2}), although even this could be improved. Any improvement which could increase the completeness of the catalogue without dramatically increasing the level of contamination should be carefully investigated. An obvious option is to include a third colour into our selection process; deep UKST r plates have recently become available in all of the NGP survey region and almost all of the SGP survey region. Fig 6.8 shows a $u - b_{\rm J}$ vs. $b_{\rm J} - r$ diagram for the f411 field which contains many previously known QSOs. The magnitude limits used are $18.25 < b_{\rm J} < 20.75$, the brighter faint limit is used because of the r plate limit of $r \sim 21$. Of the 153 known QSOs which we detect in our stellar catalogue, only 123 (80%) are selected using the standard $u - b_{\rm J} \leq -0.36$ selection, while introducing a second selection criterion based on both colours can increase this number to 142, that is, 93% completeness. It is clear that a multi-colour selection can select QSOs which have $u - b_{\rm J}$ colours which are close to the stellar locus. The addition of a third band effectively reduces the scatter from photometric errors and variability, while also constraining the stellar locus into a smaller area on the colour-colour

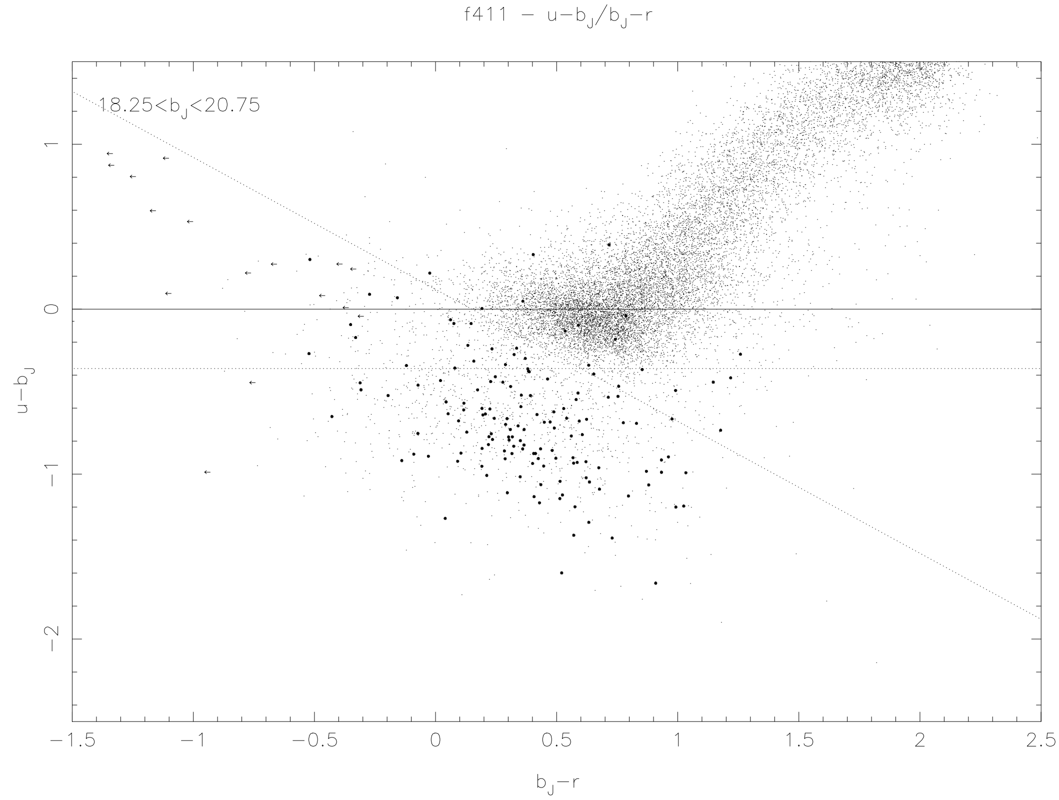

Figure 6.8: A test of QSO selection using a multi-colour selection in the f411 field, all stellar objects in the range $18.25 < b_{\rm J} < 20.75$ are marked. Known QSOs are indicated with large points, and arrows indicate upper limits on r magnitudes. The dotted lines indicate two selections, the horizontal line showing the $u - b_{\rm J} \leq -0.36$ UVX selection and the diagonal line shows a colour selection chosen to lie blueward of the stellar locus.

plane than is possible on the colour-magnitude plane. Hence, QSOs are less likely to be scattered into the stellar locus. The number density of candidates is still only at the level of 63 per deg^2 (this density includes objects with only upper limits in the r band). This would allow us, at a limiting magnitude of $b_{\rm J} \sim 20.75$, to obtain high completeness, while still retaining a low contamination rate of $< 50\%$. The loss in QSOs due to a limit 0.25 mag brighter is more than compensated for by the increased completeness. Based on the results so far obtained, we intend to extend the test observations of the 2dF QSO survey to objects which have been selected by this multi-colour process, and hence continue to improve the quality of the 2dF QSO Survey input catalogue.